IEEE Sensors Council

Embedding Fiber Bragg Grating Sensors in Carbon Composite Structures for Accurate Strain Measurement

Massimiliano Gabardi, Lorenzo Tozzetti[ID], Stefano Faralli[ID], *Member, IEEE*, Massimiliano Solazzi, David Benedetti, Samina Rajbhandari, *Student Member, IEEE*, Gianni Buttaro, and Fabrizio Di Pasquale[ID]

Abstract—Fiber Bragg grating (FBG) sensors written by femtosecond laser pulses in polyamide-coated low bending loss optical fibers are successfully embedded in carbon composite structures, following laminating and light resin molding processes which optimize the size of each ply to address esthetic, drapability, and structural requirements of the final components. The sensors are interrogated by a tunable laser operating at around 1.55 μm, and their response to temperature and strain variations is characterized in a thermally controlled chamber and by bending tests using suspended calibrated loads and a laser scanning system. Experimental results are in good agreement with simulations, confirming that the embedding process effectively overcomes potential issues related to FBG spectral distortion, birefringence, and losses. In particular, the effects of the composite material nonhomogeneity and FBG birefringence are investigated to evaluate their impact on the monitoring capabilities. A bimaterial mechanical beam model is proposed to characterize the orthotropic laminates, pointing out better accuracy in estimating the applied load with respect to the classical homogeneous beam model. A comparative analysis, performed on different instrumented carbon composite samples and supported by theory, points out the repeatability of the FBG sensors' embedding process and the effectiveness of the technology for real-time accurate strain measurement. Based on such measurements, damages and/or changes in local stiffness can be effectively detected, allowing for structural health monitoring (SHM) of composite structures for applications in specific industrial fields such as automotive and aerospace.

Index Terms— Composite materials, fiber Bragg grating (FBG), optical fiber sensors.

Massimiliano Gabardi, Lorenzo Tozzetti, Stefano Faralli, Massimiliano Solazzi, and Fabrizio Di Pasquale are with the Institute of Mechanical Intelligence, Scuola Superiore Sant'Anna, 56127 Pisa, Italy (e-mail: massimiliano.gabardi@santannapisa.it).

David Benedetti is with Carbon Dream S.p.A., 50028 Florence, Italy.

Samina Rajbhandari is with the Department of Electrical and Photonics Engineering, Technical University of Denmark (DTU), 2800 Kongens Lyngby, Denmark.

Gianni Buttaro is with Stato Maggiore Marina, 48100 Rome, Italy.

I. INTRODUCTION

FIBER optic sensors are attracting a great deal of attention for measuring many physical and bio-chemical parameters, with a wide range of industrial applications in strategic fields such as railways, automotive, aerospace, energy, oil and gas, structural health, and environmental monitoring. In particular, fiber Bragg grating (FBG) sensors [1], combined with suitable transducers, provide a reliable and effective technology for measuring physical parameters such as strain, temperature, vibration, pressure, load, torque, to mention some of them. They offer great advantages with respect to standard electronic sensors, such as small size, immunity to electromagnetic interference, robustness to harsh environment, high multiplexing capabilities providing quasi-distributed sensing, and also possible nondestructive integration in different

materials, paving the way to the new field of smart structures [2], [3]. In particular, combined progresses in FBG and composite material technologies offer engineers the possibility of integrating a fiber optic smart nervous system in composite carbon structures for real-time structural health monitoring (SHM) based on reliable quasi-distributed strain measurements within the structures [4]. Composite materials find today large use in the automotive, aerospace, naval, turbo-machines, and sport sectors. Their low density, high stiffness and strength, great resistance to wear, corrosion, and temperature make them particularly attractive. However, in such applications, the composite structures are often subject to harsh conditions, characterized by high loads, which can lead to delamination of the internal layers of the composite not observable by visual inspection. Unfortunately, other inspection techniques based on ultrasound tests or radiography are expensive, time-consuming, and not able to identify damages within the laminates on the field and in real-time [5]. On the other hand, embedding FBG sensors in composite materials makes real-time SHM techniques possible; different approaches can be implemented based on reliable strain measurement within the structures. In particular, new internal strain distributions can be identified in a composite structure as a consequence of damage, or damages can be detected by strain mapping, looking at changes in the local stiffness [4]. Note that due to the small size and lightness of the sensors, they do not alter the mechanical properties of the structures and can effectively prevent catastrophic events by monitoring the structural integrity of several key components in critical structures, as for example in aircrafts.

In this article, we integrate FBG sensors, written by femtosecond laser pulses in polyamide-coated low bending loss optical fibers, in carbon composite structures which are then mechanically and thermally characterized. The proposed technique is optimized to overcome the main issues related to the embedding process such as FBG spectral distortion, birefringence, and induced losses [6]. SHM requires an optimal characterization of both the material and the statics/dynamics of the structures to correctly estimate loads and deformations by relying on reliable local strain measurements. Thus, mechanical characterization of carbon fiber samples has been performed by loading with calibrated weights a cantilever at its tip. The experimental conditions of negligible dynamics together with a well-known static problem allow to characterize both the adopted material and the integration process parameters such as the strain transfer coefficient between FBG and composite matrix. It is known from the scientific literature that composite materials such as glass fiber and carbon fiber show different Young modulus when pulled or compressed [7], [8]; for this reason, a novel bimaterial mechanical model is proposed to characterize the orthotropic laminates in the loaded cantilever problem where both compression and traction occur at the same time in the material. The bimaterial models have been already studied in literature, but they are usually related to composites physically obtained by mating different materials [9], [10]. In the proposed study, since the mechanical properties of the material are related to its stress direction, the interface between the materials in the

model is unknown and related to both the statics and the dynamics of the problem. Moreover, accuracy in estimating the applied load obtained by adopting different material models has been compared showing that the proposed bimaterial beam model better performs with respect to the classical homogeneous beam model. Finally, the experimental results demonstrate the repeatability of the FBG sensors' embedding process and the effectiveness of the technique for accurate strain measurement to be used for real-time SHM. The strain transfer coefficients are calculated for several carbon composite samples considering their nonhomogeneity and FBG birefringence.

II. FBG Sensors' Integration in Carbon Composites

A. FBG Sensors

In its simplest form, an FBG sensor is obtained by a periodic refractive index modulation inscribed in the optical fiber core through photosensitivity or by femtosecond direct laser writing. The FBG-based sensors exploit the resonant condition induced by such periodicity, which reflects the incident light in a narrow bandwidth, with peak reflectivity at the so-called Bragg wavelength λ_B, defined as $\lambda_B = 2\,n_{\text{eff}}\Lambda$, where n_{eff} is the effective refractive index of the fundamental optical fiber mode, and Λ is the grating pitch.

The changes in both n_{eff} and Λ, induced by strain and temperature variations, will change λ_B according to

$$\frac{\Delta\lambda_B}{\lambda_B} = k\epsilon + \alpha_T\Delta T \tag{1}$$

where $\Delta\lambda_B$ is the change in the Bragg wavelength λ_B, k is the gauge factor, and α_T is the thermo-optic coefficient; the Bragg wavelength shift depends linearly on the longitudinal strain ϵ and temperature change ΔT, with sensitivity values of approximately 1.2 pm/$\mu\epsilon$ and 11 pm/°C for silica fibers at around 1550 nm. The cross-sensitivity between strain and temperature can be an issue for static strain measurements while it can be ignored for dynamic strain measurement at frequency greater than a few Hz. Also, the coating of the fiber affects the strain transfer in materials. In this article, short FBG sensors are directly written by femtosecond laser pulses [11] in polyamide-coated low bending loss optical fiber, to ensure efficient strain transduction and high-temperature operation (up to 300 °C) when embedded in the composite, also avoiding spectral distortion of the FBG spectrum.

Note that FBGs are fabricated by point-by-point direct writing by carefully optimizing the setup parameters to have first-order gratings with length 3 mm and pitch Λ of the order of 500 nm (a Bragg wavelength of 1551.05 nm has been achieved with $\Lambda = 536$ nm).

Although the strain error induced by temperature variations can be effectively compensated using a strain-free reference FBG, in the following experiments we perform static strain characterizations in laboratories at room constant temperature. The sensors are interrogated using the Hyperion reading unit from Luna Technologies, USA, based on a depolarized tunable laser [12].

B. Embedding FBG Sensors in Carbon Composites

Embedding FBG sensors in carbon composite structures allows for accurate strain measurement and then for real-time monitoring of their structural integrity as reported in [4]. Also, the manufacturing process can be monitored during different fabrication steps. Several studies have demonstrated that embedding optical fibers in carbon composite materials, along suitable directions with respect to the carbon fibers, does not alter their mechanical properties, keeping unchanged their strength and stiffness characteristics [13], [14]. The integration process requires a first definition of composite characteristics in terms of the number of plies, their thickness, and the relative carbon fiber orientation. Once defined the plybook, we select the plies among which the optical fiber including FBG sensors will be inserted, taking into account that to maximize the strain response of the sensors will require inserting the fiber as far away as possible from the plane of symmetry of the laminate. The right positioning of the sensors is controlled using a red laser light which is coupled to the optical fiber and diffused by the FBG sensors. When all the plies have been properly laid down, respecting the defined orientation of the carbon fibers, a vacuum packing is inserted in the autoclave for the curing process at suitable temperatures and pressures values for polymerization of the thermosetting epoxy matrix. Note that we have controlled the orientation of the grating with respect to the plies planes as reported in Tables I, IV, and V. The fiber has been kept in a fixed direction while the plies' orientation has been changed to achieve different configurations reported in the tables. As an example, Table I reports the plybook description of a carbon composite structure in which an FBG sensor is inserted between the third and fourth plies along the neutral axis. The table also reports the used material codes and the angles among different layers. To check the successful embedding process and the compatibility of the optical fiber with the fabrication process, we have cut the sample and took digital microscope picture of the cross section including the optical fiber. Fig. 1 shows the position of the fiber within the composite; the fiber diameter has been measured to be 140 μm, which well compares with the 155-μm specification before the integration. We can clearly observe a compression of the fiber due to the integration process without, however, noting any air bubble or discontinuity of the matrix around the optical fiber section.

To verify the effectiveness of the integration process, we have reported in Fig. 2 the FBG spectra, measured on the optical spectrum analyzer, before and after integration. Also, Table II reports the FBG characteristics before and after the integration process in terms of Bragg wavelength and FWHM bandwidth. We can clearly see that the fiber compression induced by the integration process leads to a Bragg wavelength shift of 0.55 nm to longer wavelength, also associated with a limited deformation of the FBG spectrum, with a small change in the FWHM of approximately 0.04 nm. The results reported in Fig. 2 and Table II confirm that the FBG reflection peak remains clearly defined and measurable, demonstrating a successful integration process. Note that the observed wavelength shift depends on the specific used material and integration process; however, it is repeatable and can be considered in the

TABLE I
COMPOSITION PHASES OF THE $\pm 45°$ SAMPLES WITH FBG SENSOR BETWEEN THIRD AND FOURTH PLIES

| PHASE NR.	PLY NR.	MATERIAL	ANGLE	NOTES
1	1	GG200 P 125 3K TC E3 150N2 42% – F11171000252	+/- 45°	PLY POSITIONING
2	1	GG630 TZH E3-150 N2 – F11171000028	0°/90°	PLY POSITIONING
3	1	GG630 TZH E3-150 N2 – F11171000028	0°/90°	PLY POSITIONING
4	-	FBG FIBER OPTICS	-	FBG POSITIONING
5	1	GG630 TZH E3-150 N2 – F11171000028	0°/90°	PLY POSITIONING
6	1	GG630 TZH E3-150 N2 – F11171000028	0°/90°	PLY POSITIONING
7	1	GG200 P 125 3K TC E3 150N2 42% – F11171000252	+/- 45°	PLY POSITIONING
8	-	-	-	CURING CYCLE
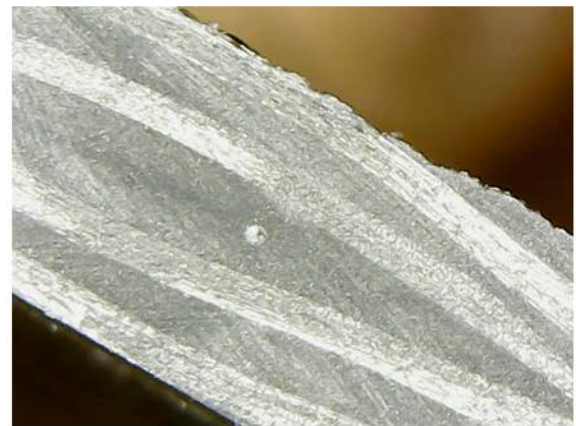
Fig. 1. Section of the carbon composite with optical fiber embedded between third and fourth plies along the neutral axis.

TABLE II
FBG CHARACTERISTICS BEFORE AND AFTER THE INTEGRATION PROCESS IN THE CARBON COMPOSITE STRUCTURE DESCRIBED IN TABLE I

FBG 04/21 C	Bragg wavelength (nm)	FWHM (nm)	R(%)
before integration	1551.05	0,52	66.4
after integration	1551.6	0,56	41.9
difference	0.55	0,04	24.5

sensor system design. Also note that short FBG sensors have been fabricated (less than 3 mm) to avoid significant spectral distortion and multipeaks' formation, as reported in [6]. The FBG reflectivity is reduced from 66.4% to 41.9% due to the integration process.

C. Characterization of the FBG Sensor Birefringence and its Impact on Sensing Performance

It is well-known that FBG sensors written by femtosecond laser pulsed are characterized by much stronger resistance to
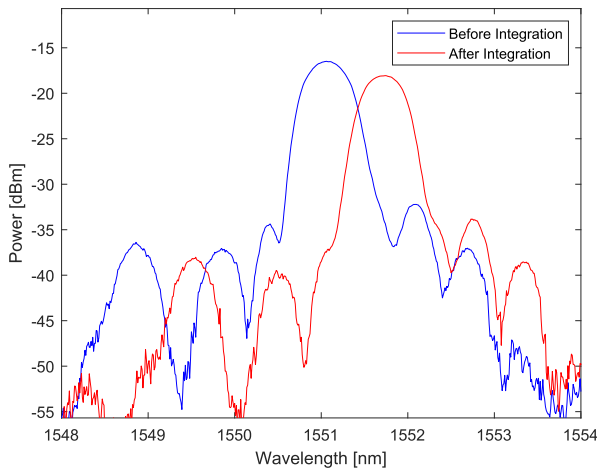
Fig. 2. Spectra of the FBG sensor integrated in the carbon composite structure described in Table I, before and after the integration process.
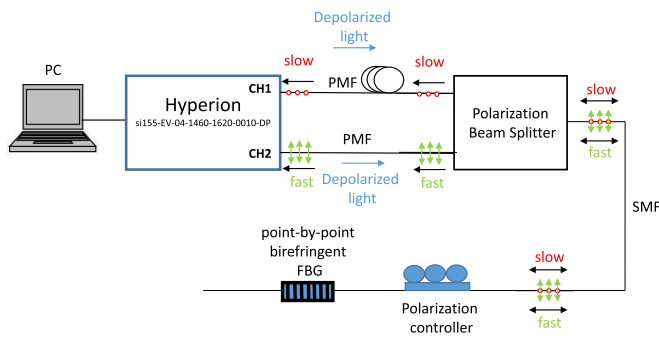

Fig. 3. Experimental setup for FBG birefringence characterization.

harsh environmental conditions with respect to FBG sensors written by exploiting photosensitivity to UV light, in particular in terms of high-temperature values and radiation doses [15], [16]. However, femtosecond direct laser writing may induce higher birefringence in the FBG response which can negatively affect the sensor accuracy [6]. Although birefringent FBG sensors, characterized by two separate peaks in the reflection bandwidth along the slow and fast axis, can be used to eliminate their temperature-strain cross-sensitivity [17] and also to measure shear stress in specific applications [18], the spurious birefringence induced by the fabrication process can be a detrimental effect, in particular when polarized light is used for their interrogation. For these reasons, we have characterized the birefringence of the fabricated FBG sensors before and after the integration process in the carbon composite structures. The experimental setup used for this characterization is described in [19] and schematically shown in Fig. 3.

Two channels of the FBG interrogator Hyperion si155-EV-04-1460-1620-0010-DP, from Luna Technologies, were used for polarization-resolved measurements. The light emitted by the tunable laser and coupled to the two channels (from left to right in Fig. 3) is characterized by a low degree of polarization (DOP). On one of the channels a 150-m-long fiber delay line was added, longer than the coherence length of the tunable laser, to provide two independent linearly polarized tunable lights at the common port of the polarization beam splitter (PBS) used to combine the two channels. Note that the light

source spectral width Δf is 1.5 MHz, and the source coherence length is approximately 130 m. The PBS shown in Fig. 3 is a micro prism device which is coupled to two polarization maintaining fibers (PMFs) and to a standard single-mode fiber (SMF) in the common port. The combined light coupled to the SMF is made of two components propagating from left to right in Fig. 3, of which one is s-linearly polarized (perpendicular to the plane of reflection of the PBS) while the second one is p-linearly polarized (parallel to the plane of reflection of the PBS). The combined beam is used to interrogate an FBG sensor written by femtosecond laser pulses (FBG length: 3 mm, pitch $\Lambda = 536$ nm, reflectivity: 66.7%). The light reflected by the FBG is split again by the PBS allowing simultaneous interrogation of the fast and slow axes of the FBG independently. Channel 1 represents the slow axis response while channel 2 the fast axis response. The light spectra reflected by the FBG enter the PBS from right to left in Fig. 3 and are then separated into fast and slow components. The two measured spectra are analyzed on the polarization controller (PC) to provide the slow and fast axis Bragg wavelengths ($\lambda_{B,\text{slow}}$ and $\lambda_{B,\text{fast}}$), determined by fitting both the reflection spectra. Note that a manual PC, shown in Fig. 3, was placed in front of the FBG to control the polarization state of the light to separate the fast and slow modes as much as possible. This allows us to measure the maximum FBG birefringence.

The birefringence parameter for standard SM fiber can be defined as $B = n_{\text{eff,slow}} - n_{\text{eff,fast}} = \lambda/L_B$, where $n_{\text{eff,slow}}$ and $n_{\text{eff,fast}}$ are the effective indices on the slow and fast axes, λ is the light wavelength, and L_B is the beat length. The Bragg wavelengths for the slow and fast axes of birefringent FBG sensors can be defined as $\lambda_{B,\text{slow}} = 2n_{\text{eff,slow}}\Lambda$ and $\lambda_{B,\text{fast}} = 2n_{\text{eff,fast}}\Lambda$, where Λ is the grating periodicity. For an FBG sensor, the Bragg reflection peaks' separation between slow and fast optical axes can be expressed as $\Delta\lambda_{f,s} = \lambda_{B,\text{slow}} - \lambda_{B,\text{fast}} = 2B\Lambda$, providing a good description of the FBG birefringence. The birefringence of the FBG inscribed in a standard single mode (SM) optical fiber by point-by-point femtosecond laser writing can then be easily observed by plotting the two spectra corresponding to the fast and slow modes, as reported in Fig. 4. Note that the measured Bragg wavelength difference $\Delta\lambda_{f,s}$ of 0.16 nm is higher than in FBG sensors written by UV light exposure (typically less than 0.1 nm). This is likely due to the highly localized and elliptical refractive index modulation induced in the fiber core by the point-by-point direct femtosecond laser writing.

Fig. 5 shows a comparison of the FBG spectra along the slow and fast axes, before and after the embedding process in a carbon composite structure. We can clearly see that the embedding process shifts both the Bragg wavelength peaks on the slow and fast axes to higher values, also increasing the FBG birefringence from 0.16 to 0.26. The increased birefringence observed after the integration process can be explained considering that the induced fiber compression increases the ellipticity of the refractive index modulation spots along the fiber core.

Table III shows a comparison among the Bragg wavelength peaks along fast and slow axes and their separation before and
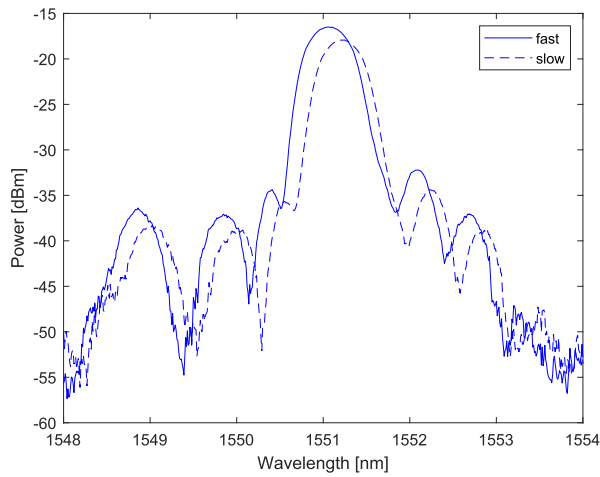
Fig. 4. FBG spectra along the fast and slow axes (the Bragg wavelength separation is 0.16 nm).
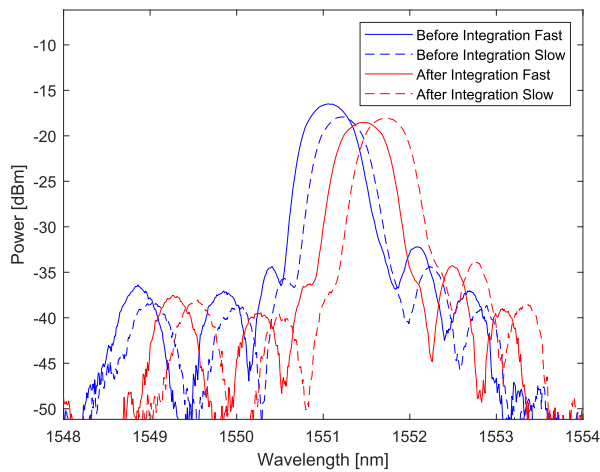

Fig. 5. FBG spectra along the fast and slow axes before and after integration in a carbon composite structure.

TABLE III
COMPARISON AMONG THE BRAGG WAVELENGTH PEAKS ALONG FAST AND SLOW AXES AND THEIR SEPARATION BEFORE AND AFTER THE INTEGRATION PROCESS

	Before integration	After integration	Wavelength shift
Peak (fast axis)	1551.05	1551.45	0.39
Peak (slow axis)	1551.21	1551.71	0.40
Peak separation	0.16	0.26	0.1

after the integration process. Several FBG sensors, written by femtosecond laser pulses and embedded in carbon composite structures, have been characterized confirming the observed behavior in terms of birefringence. We can then conclude that the higher birefringence of FBG sensors written by femtosecond laser pulses and the additional birefringence due to the integration process in composite structures require attention. The use of suitable reading unit using depolarized light sources, like the Hyperion product si155-EV-04-1460-1620-0010-DP, which provides a low DOP option, will overcome

Fig. 6. Structures of carbon composite samples with FBG sensor embedded close to the surface of the laminate (left) and along its neutral axis (right).

TABLE IV
COMPOSITION PHASES OF THE ±45° SAMPLES WITH FBG SENSOR BETWEEN FIRST AND SECOND PLIES

PHASE NR.	PLY NR.	MATERIAL	ANGLE	NOTES
1	1	GG200 P 125 3K TC E3 150N2 42% − F11171000252	+/- 45°	PLY POSITIONING
2	-	FBG FIBER OPTICS	-	FBG POSITIONING
3	1	GG630 TZH E3-150 N2 − F11171000028	0°/90°	PLY POSITIONING
4	1	GG630 TZH E3-150 N2 − F11171000028	0°/90°	PLY POSITIONING
5	1	GG630 TZH E3-150 N2 − F11171000028	0°/90°	PLY POSITIONING
6	1	GG630 TZH E3-150 N2 − F11171000028	0°/90°	PLY POSITIONING
7	1	GG200 P 125 3K TC E3 150N2 42% − F11171000252	+/- 45°	PLY POSITIONING
8	-	-	-	CURING CYCLE

the issue related to FBG birefringence, providing acceptable wavelength resolutions (10 pm for the used interrogator).

III. PRELIMINARY VALIDATION OF THE SENSING SYSTEM INTEGRATION

In this section, we report both the mechanical and thermal responses of FBG sensors embedded in a composite sample when applying mechanical loads and temperature variations. The tests aim to assess the quality of the integration procedure by checking the expected linearity between applied load and measured data in the following two cases: strain versus applied mechanical load and Bragg wavelength versus applied thermal load.

A. Smart Samples' Description

For the mechanical tests, we have considered two samples, whose structures are reported in Fig. 6, with FBG sensors embedded in the first case as far away as possible from the plane of symmetry of the laminate, while in the second one as close as possible to its neural axis. The fiber coating is polyamide to maximize the strain transfer and to allow sensor operation at higher temperature with respect to acrylate coating. The plybook sequences of the adopted samples are described in Tables I and IV. Thermal tests have been conducted only on the laminate shown in Fig. 6 left, with FBG sensor embedded far away from its plane of symmetry.

Fig. 7. Experimental set-p for mechanical characterization using calibrated loads.

B. FBG Response to Mechanical Loads

We performed cantilever-like tests with suspended calibrated loads according to gravity, as shown in Fig. 7. Fig. 8(a) and (b) reports the measured and calculated strain values versus applied loads for the two samples. We have estimated a strain sensitivity variation of $\pm6\%$ to sample thickness uncertainty of ±0.1 mm and of $\pm4\%$ to uncertainty of ±0.05 mm in the distance from the neutral axis. From the comparison between theory and experiment, we can estimate a strain transfer coefficient in Fig. 8(a) of approximately 80%. Fig. 8(b) confirms that the measured strain versus applied loads is compatible with an error of ~0.06 mm in positioning the FBG on the neutral axis. Note that the theoretical results reported in Fig. 8(a) and (b) are based on the classical homogenous Euler–Bernoulli beam theory.

C. FBG Response to Thermal Loads

We have also characterized the thermal response of the sample described in Fig. 6 left by changing its temperature from $-20\,°C$ and $+70\,°C$. Fig. 9 reports the Bragg wavelength shift induced by temperature changes, pointing out a sensitivity of 11.5 pm/°C. The thermal response of the FBG has also been characterized before integration keeping the fabricated grating loose, providing a temperature sensitivity of 10.5 pm/°C. Note that different thermal expansion coefficients of different materials can largely affect the temperature sensitivity of the embedded FBG sensors. This is not the case of carbon composite structures as the high stiffness of the material leads to low thermal expansion. We have, however, observed that in other materials, like in glass fiber structures, the FBG temperature sensitivity can significantly change after integration. Accurate static strain measurements in real applications would anyway require the use of a strain-free reference FBG to
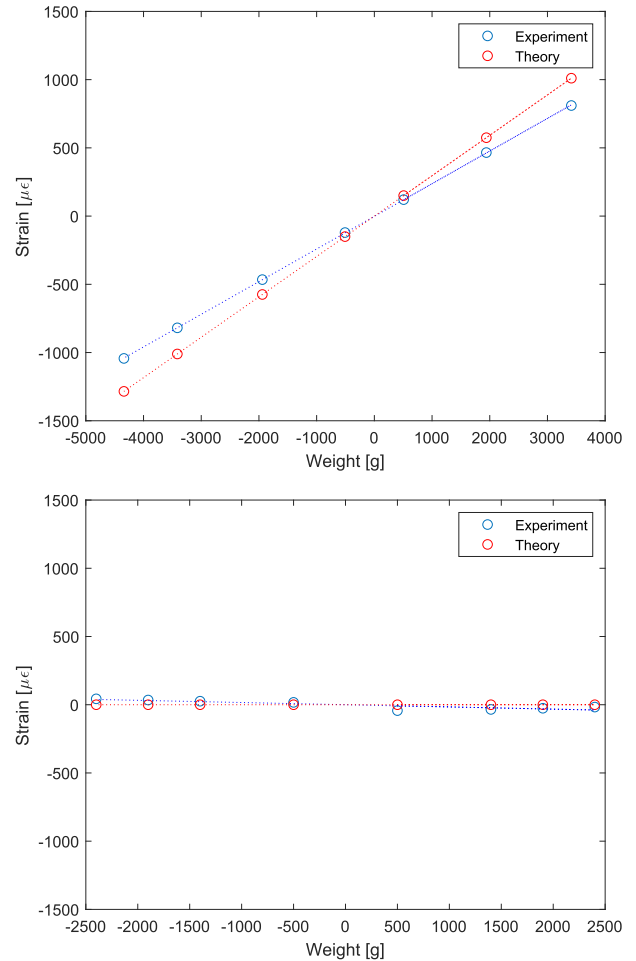

Fig. 8. Experimental and theoretical strain values versus applied loads for the samples left (top) and right (bottom) described in Fig. 6.
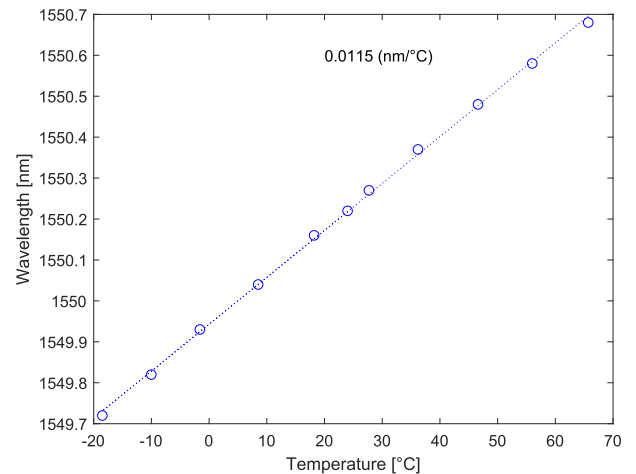

Fig. 9. FBG Bragg wavelength versus temperature.

eliminate the strain and temperature cross-sensitivity. The FBG sensor embedded along the neutral axis, described in Fig. 6 right, shows the same temperature sensitivity.

IV. MECHANICAL MODEL

Composite laminates having both a plybook symmetric with respect to the middle height plane and reinforcement fibers placed with $\theta/-\theta$ angles' orientation usually behave like
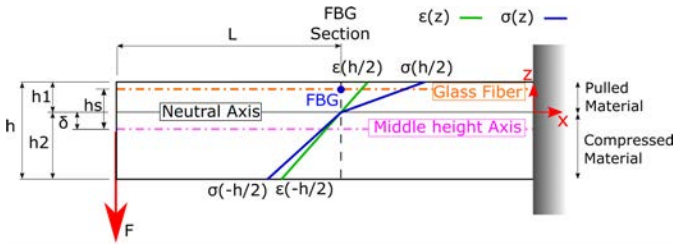
Fig. 10. Loaded cantilever experimental scheme. The beam is divided along the neutral axis; moreover, embedded glass fiber and beam middle height axis are shown. According to the bimaterial beam model, in the FBG beam section, distributions of stress σ and strain ϵ are represented.

orthotropic plates. This kind of laminates shows decoupled curvature–strain deformation effects in the middle height plane. Since carbon fiber composite material shows different stiffness when pulled or compressed, in bending tests, carbon fiber laminates show coupled curvature–strain deformation effects also when the laminates have a symmetric plybook. Such a deformation coupling is due to a shift of the neutral plane. For this reason, in this work we propose a bimaterial beam model to properly describe the carbon fiber sample behavior in a loaded cantilever test. Data acquired during the bending tests have been used to tune and validate the bimaterial beam model. Separation between the two materials is supposed coincident with the neutral axis of the samples. Fig. 10 schematically shows the statics of the performed test considering the sample as a bimaterial beam of section $b \times h$, loaded by a force F at the tip. h_1 and h_2 represent the thickness of the pulled and compressed material of the beam, respectively, and L is the distance between the applied load and the beam section where the FBG sensor has been integrated at h_s height from the middle height axis. Pulled and compressed carbon fiber composite material is featured by different Young moduli, E_1 and E_2, respectively, thus considered as two different materials. According to the Euler–Bernoulli beam theory, deformed sections will keep planar and perpendicular to the neutral axis. Due to the difference between E_1 and E_2, the neutral axis moves from the middle height axis of the δ distance. By placing a reference system with $z = 0$ on the neutral axis, such a deformation hypothesis leads to a linear distribution of strain $\epsilon(z)$ with $\epsilon(0) = 0$, as shown in Fig. 10 for the FBG section. For each of the bimaterial beam section, the $\sigma(z)$ distributions are obtained by multiplying $\epsilon(z)$ by the corresponding Young modulus. Once defined $|\sigma(h/2)| = \sigma_1$, and $|\sigma(-h/2)| = \sigma_2$, the distribution of $\sigma(z)$ can be written as follows:

$$\sigma(z) = \begin{cases} \sigma_1 \dfrac{z}{h_1}, & \text{if } z \geq 0 \\ \sigma_2 \dfrac{z}{h_2}, & \text{if } z < 0. \end{cases} \tag{2}$$

Generic equilibrium equations of the beam part between the applied load and the FBG section are reported in the following equation:

$$\begin{cases} M_y = FL = b \displaystyle\int_{-h_2}^{h_1} z\sigma(z)dz \\ F_x = 0 = b \displaystyle\int_{-h_2}^{h_1} \sigma(z)dz \end{cases} \tag{3}$$

where M_y is the bending moment, F is the applied load along z, at distance L from the FBG sensors, and b is the width of the $b \times h$ cantilever section.

By substituting and solving (2) and (3), (4) is obtained

$$\begin{cases} \dfrac{\sigma_1 h_1^2}{3} + \dfrac{\sigma_2 h_2^2}{3} = \dfrac{FL}{b} \\ \dfrac{\sigma_1 h_1}{2} - \dfrac{\sigma_2 h_2}{2} = 0. \end{cases} \tag{4}$$

According to the relation $\epsilon = \sigma/E$, (4) can be solved to obtain the relations reported in (5), where $\epsilon_1 = |\epsilon(h_1)|$ and $\epsilon_2 = |\epsilon(-h_2)|$:

$$\begin{cases} \epsilon_1 = \dfrac{3FL}{bhh_1 E_1} \\ \epsilon_2 = \dfrac{3FL}{bhh_2 E_2}. \end{cases} \tag{5}$$

Because of the known distribution of the strain in the material section, δ can be finally derived from ϵ_1 and ϵ_2 according to the following equation:

$$\delta = \frac{h\epsilon_2}{\epsilon_1 + \epsilon_2} - \frac{h}{2}. \tag{6}$$

Equivalent stiffness E_{eq} of the sample, supposed made of an homogeneous material having the same Young modulus when pulled or compressed, can be derived imposing the same displacement at the tip of the beam when the cantilever is loaded by the same load. Since the interface between the compressed and pulled material is by definition on the neutral axis, no mechanical action is exchanged at the interface. The beam part where $\sigma > 0$ can be considered as a standalone beam (Beam 1), where each section is rotating around its edge placed on the neutral axis and loaded with $F_1 < F$. Analogously, the beam part where $\sigma < 0$ (Beam 2) can be considered as a standalone beam loaded with $F_2 < F$. F_1 and F_2 verify the relation $F_1 + F_2 = F$. Since Beam 1, Beam 2, and the equivalent beam should have the same displacement when loaded with F_1, F_2, and F respectively, relation 7 represents such deformation hypothesis

$$\frac{F_1 a^3}{3E_1 I_1} = \frac{F_2 a^3}{3E_2 I_2} = \frac{F a^3}{3E_{\text{eq}} I} \tag{7}$$

where $I_1 = (bh_1^3/3)$, $I_2 = (bh_2^3/3)$, and $I = (bh^3/12)$ are the second moment area, and a is the distance between the fixed support of the cantilever and the applied load F on the beam.

Equation (7) can be used together with $F_1 + F_2 = F$ to obtain (8), where E_{eq} is derived as a function of both the material stiffnesses E_1 and E_2

$$E_{\text{eq}} = \frac{4\left(E_1 h_1^3 + E_2 h_2^3\right)}{h^3}. \tag{8}$$

Previously mentioned equations define the relations between the applied load and both the strain and stress distributions in a cantilever, under the hypothesis of a material constitutive model where the young modulus is different when the material is pulled or compressed.
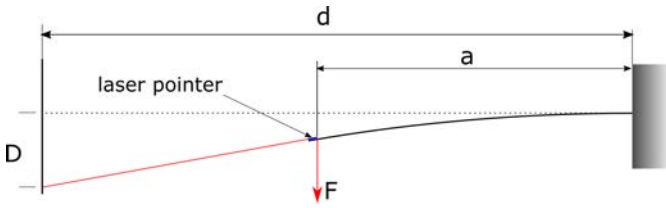
Fig. 11. Scheme of the deformed beam and laser pointer setup. "D" measure (taken on the left wall) is used to experimentally derive the equivalent stiffness of the sample.

V. Theoretical and Experimental Results

A. Comparative Analysis on Different Samples

1) Experiment Description: To evaluate the integration process repeatability and the effectiveness of the FBG technology for accurate strain measurement to be used for real-time SHM of composite structures [4], we have performed a comparative experimental analysis, supported by theory, on different instrumented composite samples. Six different carbon composite samples made with two different plybooks have been fabricated embedding femtosecond laser written FBG sensors on polyamide low bending loss fiber, as close as possible to the external surface of the laminate to maximize the strain response. All the six samples have been characterized twice with the cantilever beam test previously described: first time placing the FBG on the ceiling side (traction condition) and second time by turning the sample with respect to the gravity load and placing the FBG on the floor side (compression condition). According to Fig. 11, a laser pointer placed on the tip of the cantilever and positioned to keep tangent to the cantilever end has been used to derive the loaded cantilever deformation D. In each trial, seven different loads have been applied and seven independent load–strain–deformation measurements have been performed. Such deformation measurements have been used to derive the equivalent stiffness E_{eq} of each sample. Equivalent stiffness values are obtained from the deformation measurements by solving the geometrical relation described by (9), where $(Fa^3/3E_{eq}I)$ and $(Fa^2/2E_{eq}I)$ represent the vertical displacement and the rotation of the beam section where the load is applied, respectively, while d is the distance between the vertical wall where the laser light is projected and the cantilever fixed constraint. E_{eq} has been obtained for each of the applied loads. The mean value between the equivalent stiffness values, associated with each of the measured laser pointer displacement, has been assumed as the equivalent stiffness of the sample (E_{eq})

$$\frac{D - \frac{Fa^3}{3E_{eq}I}}{\tan\left(\frac{Fa^2}{2E_{eq}I}\right)} - (d - a) = 0. \tag{9}$$

According to the mechanical model of the loaded bimaterial cantilever, described in Section IV, both the compression and traction FBG strain measures have been used to estimate for each of the seven loads, the neutral axis shift δ by means of (6) with h_s instead of h.

With reference to the measured strain, (5) can be rewritten both as A function of the derived measure of δ and taking into account a strain transfer coefficient η that estimates the

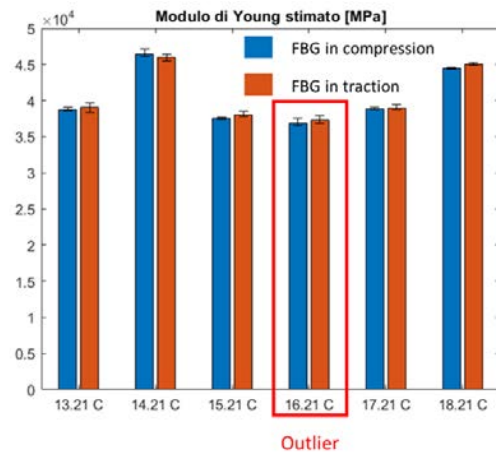| PHASE NR.	PLY NR.	MATERIAL	ANGLE	NOTES
1	1	GG200 P 125 3K TC E3 150N2 42% – F11171000252	0°/90°	PLY POSITIONING
2	-	FBG FIBER OPTICS	-	FBG POSITIONING
3	1	GG630 TZH E3-150 N2 – F11171000028	0°/90°	PLY POSITIONING
4	1	GG630 TZH E3-150 N2 – F11171000028	+/- 45°	PLY POSITIONING
5	1	GG630 TZH E3-150 N2 – F11171000028	+/- 45°	PLY POSITIONING
6	1	GG630 TZH E3-150 N2 – F11171000028	0°/90°	PLY POSITIONING
7	1	GG200 P 125 3K TC E3 150N2 42% – F11171000252	0°/90°	PLY POSITIONING
8	-	-	-	CURING CYCLE

Fig. 12. Young modulus estimated for the six samples with FBG in compression and traction.

performance of the bonding in transferring the strain from the composite material matrix to the sensing element. This leads to the following equation:

$$\begin{cases} \epsilon_1 = \dfrac{3FL}{bh\left(\frac{h}{2} - \delta\right)E_1}\dfrac{h_s - \delta}{\frac{h}{2} - \delta}\eta \\ \epsilon_2 = \dfrac{3FL}{bh\left(\frac{h}{2} + \delta\right)E_2}\dfrac{h_s + \delta}{\frac{h}{2} + \delta}\eta. \end{cases} \tag{10}$$

For each load application, (10) together with (8) can then be solved to derive numerical values of the unknown physical properties of the model E_1, E_2, and η.

2) Smart Samples' Description: Six smart samples have been used for the tests, three of them (13.21C, 15.21C, and 17.21C) have been realized according to the plybook described in Table IV and named ±45°, whereas the other three (14.21C, 16.21C, and 18.21C) have been realized according to the plybook described in Table V and named 0°/90°.
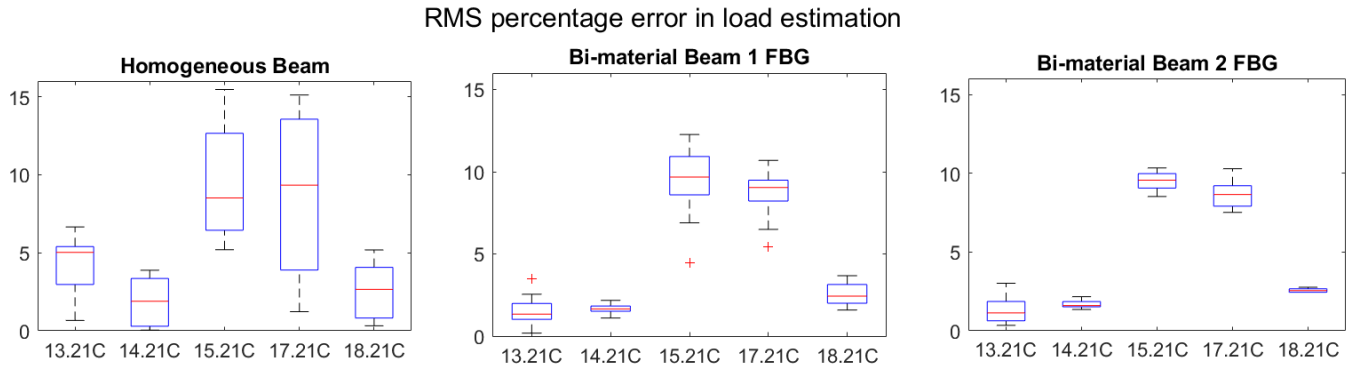
RMS percentage error in load estimation

Fig. 13. RMS of the percentage error performed in estimating the applied load obtained with the three proposed methodologies. Results are aggregated by tested samples.

B. Data Analysis

To validate the proposed sensing system for monitoring carbon fiber composite structures, load estimation has been performed by starting from strain FBG reading. Unknown constitutive parameters of the model have been assumed by averaging the values obtained for each load application. The obtained numerical values are reported in Section V-C.

Three different approaches to load estimation have been compared to validate the proposed mechanical model with respect to the classical homogeneous beam theory and determine the minimum number of embedded FBG necessary to perform load monitoring.

1) Homogeneous Beam Theory: According to the homogeneous beam theory, the relation between strain reading and load is reported in the following equation:

$$F = \frac{\epsilon E_{eq}bh^3}{12Lh_s\eta} \tag{11}$$

where ϵ represents the strain reading, and no δ shift of the neutral axis is considered. In the described condition, only a preliminary characterization of the constitutive parameters $E90_{eq}$ (or $E45_{eq}$) and η is required. Furthermore, the homogeneous beam theory only requires one FBG to perform load estimation. As described in Section V-A1, two measurements have been performed with the same loads to simulate the use of two FBGs symmetrically embedded in the laminate samples; the load F has been estimated in this case using the strain measurements performed in the two load conditions (traction/compression) independently.

2) Bimaterial Beam With One FBG: When the bimaterial beam mechanical model is adopted, it is possible to perform the load estimation with only one FBG strain sensor by performing the preliminary characterization of the constitutive parameters $E90_{eq}$ (or $E45_{eq}$), $\delta90$ (or $\delta45$), and η. Equation (12) shows the relation obtained for the described force monitoring condition

$$\begin{cases} F = \dfrac{\epsilon E_{eq}bh^3}{12L(h_s - \delta)\eta}, & \text{if } \epsilon \geq 0 \\[4mm] F = \dfrac{\epsilon E_{eq}bh^3}{12L(h_s + \delta)\eta}, & \text{if } \epsilon < 0. \end{cases} \tag{12}$$

In addition, for the bimaterial beam with only one strain measure, the load F has been estimated using the strain

measurements performed in the two load conditions (traction/compression) independently.

3) Bimaterial Beam With Two Symmetrical FBG: By substituting (6), evaluated considering the FBG sensors height h_s, into (12), (13) is obtained. Such relation shows that in the proposed load condition, by having two symmetrical measures of strain in the same sample section, only one constitutive parameter $E90_{eq}$ (or $E45_{eq}$) is required to perform the load estimation in carbon fiber laminates with the proposed bimaterial mechanical model

$$F = \frac{\epsilon E_{eq}bh^3(\epsilon_1 + \epsilon_2)}{24L(h_s)\eta}. \tag{13}$$

C. Results and Discussion

Fig. 12 shows the mean, minimum, and maximum values of the Young modulus (E) obtained for each sample in two different load cases: FBG compressed and FBG pulled. Excluding sample 16.21C that clearly represents an outlier, likely connected to the fabrication process, we have obtained $E45_{eq} = 3.8557 \cdot 10^4$ MPa for the odd samples ($\pm 45°$) and $E90_{eq} = 4.5475 \cdot 10^4$ MPa for the even samples ($0/90°$) as the mean of the equivalent stiffness values derived by solving (8) for each load application.

According to the proposed mechanical model or the classical homogeneous beam theory, by means of the three different methodologies described in Section V, the load F can be estimated as a function of the measured strain ϵ_1 (traction condition), ϵ_2 (compression condition), the correct equivalent Young modulus $E90_{eq}$ or $E45_{eq}$, the neutral axis shift δ, and the strain transfer coefficient η. Since η is a physical variable related to the interaction between the composite matrix and the glass fiber of the sensor, it has been assumed equal for both types of samples and it has been determined by averaging the values obtained for each load application performed on each of the samples, obtaining $\eta = 0.8969$. Such a high value of the strain transfer coefficient with respect to the reference values reported in the scientific literature [20] is explainable taking into account that the entire glass fiber is embedded in the samples' composite material matrix, whereas in most of the applications described in the literature FBG sensors are glued on the surfaces of the samples. Furthermore, $\delta45$ and $\delta90$ parameters have been assumed different for the

two plybooks. They have been estimated by averaging the values obtained for each load application on the odd and even samples, respectively. Values obtained are $\delta 45 = 0.048$ mm and $\delta 90 = 0.0199$ mm.

Fig. 13 shows the rms percentage error obtained by estimating the applied load by means of the three described methodologies. Note that for each tested sample, the proposed bimaterial beam theory better describes the deformation of the beam, thus allowing a better estimation of the load starting from the strain measures with respect to the classical homogeneous beam theory. Low difference in load estimation accuracy appears between the 1 FBG method and the 2 FBG method. Since in the 2 FBG method the value of δ is supposed different for each load application trial and freely depends by the measured strains ϵ_1 and ϵ_2, less measurement error is introduced in the load estimation process thus obtaining better accuracy.

VI. Conclusion

In this work, integration of FBG sensors in carbon fiber composite laminates aiming to SHM has been successfully performed. Preliminary mechanical and thermal tests have been executed on a laminate provided with sensors to validate the integration process. Successively, six samples equally divided in two groups by plybook ($\pm 45°$, $0/90°$) have been tested with a tip loaded cantilever test to verify the repeatability of the process and validate a novel mechanical model for the description of the carbon fiber laminates behavior as a material featured by different stiffness when pulled or compressed. The model has been validated by measuring the equivalent stiffness of the laminates via laser pointer in an independent way. Equivalent stiffness measure together with performed strain measures have been used to estimate the applied load on the cantilever by means of the presented mechanical model. The results show that the presented model performs better than the classical homogeneous beam theory both when applied with one FBG and when applied with two opposite FBG. Although load estimation using only one FBG is less accurate than the load estimation with two FBGs, and also requires the accurate characterization of both the compression and traction stiffness modules, it is still relevant because of the reduced number of sensors required for its application.

References

[1] A. Kersey et al., "Fiber grating sensors," *J. Lightw. Technol.*, vol. 15, no. 8, pp. 1442–1463, Aug. 1997.

[2] K. S. C. Kuang, R. Kenny, M. P. Whelan, W. J. Cantwell, and P. R. Chalker, "Embedded fibre Bragg grating sensors in advanced composite materials," *Compos. Sci. Technol.*, vol. 61, no. 10, pp. 1379–1387, Aug. 2001.

[3] Y. Fan and M. Kahrizi, "Characterization of a FBG strain gage array embedded in composite structure," *Sens. Actuators A, Phys.*, vol. 121, no. 2, pp. 297–305, Jun. 2005.

[4] A. Güemes, A. Fernández-López, P. Díaz-Maroto, A. Lozano, and J. Sierra-Perez, "Structural health monitoring in composite structures by fiber-optic sensors," *Sensors*, vol. 18, no. 4, p. 1094, Apr. 2018.

[5] S. Gholizadeh, "A review of non-destructive testing methods of composite materials," *Proc. Struct. Integrity*, vol. 1, pp. 50–57, Jan. 2016.

[6] G. Luyckx, E. Voet, N. Lammens, and J. Degrieck, "Strain measurements of composite laminates with embedded fibre Bragg gratings: Criticism and opportunities for research," *Sensors*, vol. 11, no. 1, pp. 384–408, Dec. 2010.

[7] W. Wu, Q. Wang, and W. Li, "Comparison of tensile and compressive properties of carbon/glass interlayer and intralayer hybrid composites," *Materials*, vol. 11, no. 7, p. 1105, Jun. 2018.

[8] N. Insausti, I. Adarraga, N. Carbajal, and F. Mujika, "Numerical assessment of the analytical models used to determine flexural and shear moduli in I-beams when the tensile and compressive moduli are different," *Polym. Test.*, vol. 81, Jan. 2020, Art. no. 106154.

[9] P. G. Coelho, J. M. Guedes, and H. C. Rodrigues, "Multiscale topology optimization of bi-material laminated composite structures," *Compos. Struct.*, vol. 132, pp. 495–505, Nov. 2015.

[10] A. Heidarpour and M. A. Bradford, "Generic non-linear modelling of a bi-material composite beam with partial shear interaction," *Int. J. Non-Linear Mech.*, vol. 44, no. 3, pp. 290–297, Apr. 2009.

[11] J. He, B. Xu, X. Xu, C. Liao, and Y. Wang, "Review of femtosecond-laser-inscribed fiber Bragg gratings: Fabrication technologies and sensing applications," *Photon. Sensors*, vol. 11, no. 2, pp. 203–226, Jun. 2021.

[12] *HYPERION Optical Sensing Instrument si155*. [Online]. Available: https://lunainc.com/sites/default/files/assets/files/resource-library/LUNA-Data-Sheet-Micron-si155_v3.pdf

[13] N. Takeda and S. Minakuchi, "Smart aircraft composite structures with embedded small-diameter optical fiber sensors," *Proc. SPIE*, vol. 8351, pp. 129–136, Jan. 2012.

[14] R. Ramly, W. Kuntjoro, and M. K. A. Rahman, "Using embedded fiber Bragg grating (FBG) sensors in smart aircraft structure materials," *Proc. Eng.*, vol. 41, pp. 600–606, Jan. 2012.

[15] M. A. S. Zaghloul et al., "Radiation resistant fiber Bragg grating in random air-line fibers for sensing applications in nuclear reactor cores," *Opt. Exp.*, vol. 26, no. 9, pp. 11775–11786, 2018.

[16] K. Chah, D. Kinet, M. Wuilpart, P. Mégret, and C. Caucheteur, "Femtosecond-laser-induced highly birefringent Bragg gratings in standard optical fiber," *Opt. Lett.*, vol. 38, no. 4, pp. 594–596, Feb. 2013.

[17] L. Polz et al., "Regenerated Bragg gratings in panda fibers for simultaneous temperature and force measurements at high temperatures," *J. Lightw. Technol.*, vol. 34, no. 19, pp. 4550–4556, Oct. 1, 2016.

[18] S. Sulejmani et al., "Shear stress sensing with Bragg grating-based sensors in microstructured optical fibers," *Opt. Exp.*, vol. 21, no. 17, pp. 20404–20416, 2013.

[19] P. Singh, F. Jülich, and J. Roths, "Polarization dependence of the strain sensitivity of fiber Bragg gratings inscribed in highly birefringent optical fibers," *Proc. SPIE*, vol. 8439, May 2012, Art. no. 84391S.

[20] W. Y. Li, C. C. Cheng, and Y. L. Lo, "Investigation of strain transmission of surface-bonded FBGs used as strain sensors," *Sens. Actuators A, Phys.*, vol. 149, no. 2, pp. 201–207, Feb. 2009.

Massimiliano Gabardi received the M.Sc. degree in mechanical engineering from the University of Pisa, Pisa, Italy, in 2014, and the Ph.D. (Hons.) degree in emerging digital technologies curriculum perceptual robotics from Scuola Superiore Sant'Anna, Pisa, in 2018.

In 2017, he was a Visiting Ph.D. Student with the Institut des Systèmes Intelligents et de Robotique (ISIR), University Pierre et Marie Curie (UPMC, Sorbonne Universités), Paris, France. He is a Postdoctoral Researcher with the PERCeptual RObotics Laboratory (PERCRO Lab), Institute of Mechanical Intelligence, Scuola Superiore Sant'Anna. His main research interests include human–robot interaction with a particular focus on wearable haptics, rehabilitation robotics, teleoperation and collaborative robotics, innovative sensors systems, and smart materials.

Lorenzo Tozzetti was born in Florence, Italy, in 1982. He received the bachelor's degree in physics and the master's degree in astrophysics from the University of Florence, Florence, in 2009 and 2017, respectively.

From 2009 to 2011, he worked on the production of cosmic dust analogs with the Department of Physics and Astronomy, University of Florence, as a Research Fellow. From 2011 to 2014, he was with the INAF—Astrophysical Observatory of Arcetri, Florence, as a Research Fellow, focusing on the characterization of Cosmic Dust Analogs. In the following two years, he further developed the same topics with the University of Florence. From 2016 to 2017, he was with the CNR—National Institute of Optics (INO), Florence, on the development of a prototype for the analysis of the composition of planetary atmospheres. Since 2018, he has been with TeCIP Institute, Scuola Superiore Sant'Anna, Pisa, Italy, as a Research Fellow. His research interests include optical fiber sensors and silicon photonic.

Stefano Faralli (Member, IEEE) received the M.Sc. degree in physics from the University of Pisa, Pisa, Italy, in 2000, the M.Sc. degree in optical communications systems and networks from the Politecnico di Milano, Milan, Italy, in 2001, and the Ph.D. degree in telecommunications technology from Scuola Superiore Sant'Anna, Pisa, in 2006.

From 2011 and 2012, he was a Visiting Scholar with the Optoelectronics Group, University of California at Santa Barbara, Santa Barbara, CA, USA. In the period between 2015 and 2017, he was a Senior Process Engineer with the Inphotec Center, Scuola Superiore Sant'Anna, in-charge for the processes of PECVD and LPCVD deposition, wet, and dry oxidation. He is currently an Assistant Professor with Scuola Superiore Sant'Anna. He is also the Co-Founder of Infibra Technologies S.r.l., Pisa, a spin-off company of Scuola Superiore Sant'Anna. He is the author or a coauthor of publications among patents and papers in peer-reviewed international journals and conference digests. His research interests include optical fiber sensors, integrated optics, silicon photonics, thin-film processing, and optical amplification for optical communication systems and networks.

Massimiliano Solazzi received the Ph.D. degree in innovative technologies from Scuola Superiore Sant'Anna, Pisa, Italy, in 2010.

He is currently an Associate Professor in Applied Mechanics with Scuola Superiore Sant'Anna, and carries out his research with the PERCRO Laboratory, Institute of Mechanical Intelligence. His research interests include design of robotic interfaces for virtual reality, teleoperation, and rehabilitations, design and control of arm exoskeletons, development of control systems for manipulators, and psychophysical validation of human machine interface (HMI).

David Benedetti received the degree in electronic engineering (telecommunications specialization) from the University of Pisa, Pisa, Italy, in 1998, the degree in defense and security sciences (maritime and naval sciences) from the University of Pisa, in 2003, and the master's degree in political science (international law and space law) from the University of Trieste, Trieste, Italy, in 2005.

After a 13-year military career in the Italian Navy as Line Officer, from training in the Naval Academy to assignments on board Navy warships, he has worked at SELEX Sistemi Integrati S.p.A., Rome, Italy, as a Systems Engineer for the application of the concepts of system engineering and network-centric warfare in system-level architectures for various programs in the Defense and Homeland Security sectors. He is currently with Carbon Dream S.p.A., Florence, Italy, a leading company in composite materials, as a Program Manager in Automotive business unit and the Head of the Defense and Aerospace division.

Samina Rajbhandari (Student Member, IEEE) received the Erasmus mundus joint master's degree, called Photonic Integrated Circuits, Sensors and networks (PIXNET), from Aston University, Birmingham, U.K., and Scuola Superiore Sant'Anna, Pisa, Italy, in 2021. She is currently pursuing the Ph.D. degree with the SPOC Center, Department of Photonics Engineering, Technical University of Denmark (DTU), Kongens Lyngby, Denmark.

Her research interests include signal processing techniques to implement space division-multiplexing (SDM) technology based on novel multimode fibers.

Gianni Buttaro was born in Gaeta, Italy, in 1987. He received the bachelor's degree in naval architecture and marine engineering from the Italian Naval Academy, Leghorn, Italy, in 2010, and the master's degree in naval architecture and marine engineering from the University of Genoa, Genoa, Italy, in 2013.

From 2013 to 2020, he worked aboard several navy submarines including ITS Scirè, ITS P. Longobardo, and ITS G. Prini first as an Engineer Officer and as a Chief Engineer. He attended the "Submarine Design and Acquisition Course" with University College London, London, U.K., in 2021, and he received the First Level Specializing Master in design, application, and regulation of remotely piloted aircraft systems with the University of Tor Vergata, Rome, Italy, in 2022. Since 2020, he has been with the Submarines Department, Italian Navy General Staff, as the Head of Technical and Safety Design Analysis Section, where he is responsible for contributing to definition of design studies and general technical requirements relating to new submarines, plants, equipment, and modernization of submarines in service.

Fabrizio Di Pasquale received the degree in electronic engineering from the University of Bologna, Bologna, Italy, in 1989, and the Ph.D. degree in information technology from the University of Parma, Parma, Italy, in 1993.

From 1993 to 1998, he was with the Department of Electrical and Electronic Engineering, University College London, London, U.K., as a Research Fellow, working on optical amplifiers, wavelength division multiplexed (WDM) optical communication systems, and liquid crystal displays. After two years with Pirelli Cavi e Sistemi, Milan, Italy, and two years with Cisco Photonics Italy, Vimercate, Italy, he moved to Scuola Superiore Sant'Anna, Pisa, Italy, where he is currently a Full Professor of Telecommunications with the Institute of Mechanical Intelligence. He is the Co-Founder of Infibra Technologies S.r.l., Pisa, a spin-off company of Scuola Superiore Sant'Anna, developing and marketing fiber optic sensor systems. He has filed 25 patents and is the author or a coauthor of more than 250 scientific journals and conference papers. His research interests include optical fiber sensors, silicon photonics, optical amplifiers, WDM transmission systems, and networks.

Dr. Di Pasquale has been a Technical Program Committee (TPC) member of several international conferences and on the board of reviewers of international refereed journals.